AREA OF INTEREST 2 – A SYSTEMATIC MULTISCALE MODELING AND EXPERIMENTAL APPROACH TO PROTECT GRAIN BOUNDARIES IN MAGNESIUM ALLOYS FROM CORROSION

CENTER FOR ADVANCED VEHICULAR SYSTEMS (CAVS)
MISSISSIPPI STATE UNIVERSITY

Principal Investigator: Mark F. Horstemeyer
Center for Advanced Vehicular Systems (CAVS)
Mississippi State University
206 Carpenter Bldg., PO Box ME, Mississippi State, MS 39762
Phone: (662) 325-7308; Fax: (662) 325-7223; E-mail: mfhorst@cavs.msstate.edu

Co-Principal Investigator: Santanu Chaudhuri
Illinois Applied Research Institute
Computational Science and Engineering
University of Illinois at Urbana-Champaign
2100 S Oak St., Champaign IL 61822
Phone: (509) 944-1296; E-mail: santc@illinois.edu

DOE Technology Area Development Manager : William Joost
U.S. Department of Energy
1000 Independence Avenue, S.W., Washington, DC 20585
Phone: (202) 287-6020; E-mail: william.joost@ee.doe.gov

Contractor: Mississippi State University
Contract No.: DE-FOA-0000793

Executive Summary

A multiscale modeling Internal State Variable (ISV) constitutive model was developed that captures the fundamental structure-property relationships. The macroscale ISV model used lower length scale simulations (Butler-Volmer and Electronics Structures results) in order to inform the ISVs at the macroscale. The chemomechanical ISV model was calibrated and validated from experiments with magnesium (Mg) alloys that were investigated under corrosive environments coupled with experimental electrochemical studies. Because the ISV chemomechanical model is physically based, it can be used for other material systems to predict corrosion behavior. As such, others can use the chemomechanical model for analyzing corrosion effects on their designs.

---

1. Accomplishments

- Performed geometry optimization computations within the framework of density functionals (DFT) on pure and doped Mg(0001) surfaces. Calculated the energy of segregation for the dopant metals (X=Al, Fe, Zn, Ca and Mn) from the bulk of Mg to the topmost layers of Mg(0001), along with the surface energy changes during segregation.

- Identified the preferred adsorption configuration and energetics of molecules relevant to hydrogen evolution, i.e. H2O, OH and H, on pure and doped Mg(0001) surfaces through DFT.
- Initiated and partially completed the computations on the potential dependent energetics of competitive reaction paths of electrochemical H2O decomposition, e.g. hydrogen evolution reaction, on pure and doped Mg(0001) surfaces.
- Procured pure Mg (99.95% purity), Mg-Al magnesium alloys (made from commercial pure Mg (99.95%) and commercial pure Al (99.99%) with 2 wt.%, 4 wt.%, and 6 wt.% Al), as well as Mg-Zn magnesium alloys (made from commercial pure Mg (99.95%) and commercial pure Zn (99.99%) with 2 wt.%, 4 wt.%, and 6 wt.% Zn).
- Conducted the corrosion surface characterization to investigate the corrosion properties of the procured magnesium alloys by performing preliminary electrochemical studies (quantify the hydrogen oxidation reaction, potential-dynamic polarization curve) and immersion corrosion experiments (quantify general corrosion, localized pitting corrosion, and profilometry analysis).
- Completed the formulation of the kinematics, kinetic, thermodynamics, and mass balance for the corrosion damage model.
- Lower length scale simulations were used to inform the macroscale Internal State Variable (ISV) corrosion model
- The macroscale ISV corrosion model was finalized and calibrated to magnesium with different amount of aluminum (0%, 2%, 4%, and 6%).

2. Technology Assessment

- The technology of the ISV corrosion model is now ready for engineering practice. The model has been developed, implemented, and calibrated.

3. Introduction

Aging of materials in corrosive environment has become a principal cause for the reduction in the reliability and durability of engineered systems [1-4]. Magnesium alloys as a kind of lightweight materials are getting increasing attention from automotive and aerospace industries, due to their specific high strength to weight ratio [5]. However, magnesium alloys' service life can be significantly reduced when exposed to the external environment, because of their high corrosion rate [6]. Development of an accurate constitutive model that accounts for damage progression effects from mechanical loading and corrosion is necessary.

Internal state variable (ISV) theory is a constitutive material model that can capture the history effect of materials and is widely used in continuum damage mechanics filed [7]. Coleman and Curtin [8] were the first lay out the framework of ISV theory, they used Clausius-Duhem inequality to place restriction on the response functions. Later, Gurson [9] developed a yield criteria for ductile materials including damage evolution and plasticity. Bammann [10] employed the Cocks and Ashby [11] creep void growth rule into the ISV formulism to account for the large deformation kinematics. Voyiadjis [12-14] extended the ISV damage model by coupling the kinematics, kinetics, and thermodynamics into the damage rate equations. By including damage as an ISV variable, different forms of damage rules can be easily incorporated into the constitutive framework. Horstemeyer [15, 16]

enriched the ISV damage model by accounting for the microstructure features and dividing the damage progression into void nucleation, growth, and coalescence. For the past decades, ISV theory has made a big achievement in capturing the damage evolution for materials subjected to mechanical loadings. Corrosion process can also induce damage, reduce material strength, enhance the inelastic flow, and soften the elastic moduli, but, the ISV theory was not widely applied to capture the damages caused by corrosion. Walton [17] developed a corrosion model based upon ISV theory by using an extended multiplicative decomposition of the deformation gradient that accounts for corrosion effects. Walton's ISV corrosion model has the capability to capture the macroscale damages, such as, general corrosion, pit nucleation, pit growth, pit coalescence, and intergranular corrosion.

As known corrosion is highly dependent on the alloying elements and microstructural features. During the manufacturing process, many of the grain boundaries and grain orientations may be modified. Some impurity elements/second phase may segregate from matrix, whereby they modify the corrosion stability of material. However, there is no clear knowledge on how doping and material engineering can be used favorably for altering corrosion rates in promising Mg alloys. Multiscale modeling technique provides a powerful approach to accurately model the corrosion effects by considering the dopping effects and the material microstructure-property relationships.

In the following two sections, the developed multiscale ISV inelasticity model for corrosion is explained. However, first the lower length scale simulations (due to downscaleing requirements) are presented. The larger length scale model adds the corrosion ISVs to the Bammann [10, 18, 19] and Horstemeyer [15, 20] thermomechanical plasticity model, but also relates different corrosion mechanisms (general corrosion, pitting corrosion, intergranular/filiform corrosion) to materials' microstructural features based on the corrosion framework of Walton [17]. For the ISV constitutive corrosion model part, a macroscale corrosion damage model is explained first. As the nature behind the corrosion damage was actually the anodic and cathodic reactions occurring on the material surfaces. The Butler-Volmer equation was applied to bridge the macroscale corrosion damage to the mesoscale electrochemical kinetics. The mesoscale electrochemical kinetics behaviors can be predicted by bridging Butler-Volmer equation to materials' microstructural features and nanoscale electrochemical activation energy. Second, the lower length scale first principles simulations of corrosion are presented.

4. Approach

4.1. DFT Simulations

The goal of the proposed multiscale modeling research was to establish fundamental structure-property relationships in cast magnesium (Mg) alloys by investigating critical grain boundary phenomena (intergranular failure) during corrosion coupled with experimental electrochemical studies. In FY2014, DFT computations were performed to determine the energetics and configurational aspects of hydrogen evolution and the potential dependence of reaction rates, on pure and alloyed Mg(0001) surfaces in a comparative way. Periodic slab computations within the framework of DFT were performed using VASP-PW91 on high performance computing clusters. A new consistent formulation coupling kinematics, thermodynamics, chemical mass balance, and kinetics was developed

to account for the corrosion damage by using an extended multiplicative decomposition of deformation gradient. The corrosion model, based upon internal state variable (ISV) theory, captures the effects of general corrosion, pit nucleation, pit growth, pit coalescence, and intergranular corrosion.

With respect to the mulitscale experiments, high purity level magnesium alloys (Mg-2wt.%,4wt.%, 6wt.% Al, Mg- Mg-2wt.%,4 wt.%, 6wt.% Zn) was procured, and these materials are prepared by vacuum induction melting the alloying elements in a hard-fired Coors Tek alumina crucible under an atmosphere of high purity argon. Then, the materials were casted into a water-cooled copper chill-mold forming a four inch diameter ingot with thirteen inch long. The detail chemical composition of the pure Mg and Mg-2 wt.% Al was identified by SpectroMax, and the microstructure of these two alloys was characterized under the optical microscope and scanning electron microscope (SEM). Scanning electro-chemical microscope (SECM) was applied to quantify the hydrogen evolution rate on the specimen surfaces. In addition, corrosion potential of the procured material was investigated by conducting the potential dynamic polarization tests. In addition, corrosion damages caused by general corrosion, integranular corrosion, and localized pitting corrosion were quantified by performing immersion corrosion tests and profilometry analysis.

4.1.1 First Principle design, simulation, and optimization

DFT computations aimed to find answers to the following subjects:

- Energetics of surface segregation of impurity atoms from bulk to the surface of Mg(0001)
- Effect of impurity atoms on surface energy and stability of Mg(0001)
- Effect of impurity atoms on energetics of H2O, H and OH adsorption, and H2O decomposition.

The energy of segregation of impurity atoms, X, from the bulk of Mg to Mg(0001) surface were found through substitution of an Mg atom from inner and topmost layers, in order, with X, and a following geometry optimization to calculate the change in energy. For X tried here, i.e. X=Al, Fe, Zn, Ca or Mn, the segregation energy was found to be positive except for X=Ca. It is assumed that the driving force that governs the segregation thermodynamics is the electronegativity difference between X and Mg: Ca, the only element with a lower electronegativity than Mg energetically prefers to locate at the surface, whereas the others energetically prefer to reside in the bulk. Computations also revealed that Fe and Mn doping causes magnetization in the alloy.

To understand the effect of impurity segregation on the surface stability of Mg(0001), the surface energy, E_{surf} , before and after doping, i.e. of Mg(0001) and MgX(0001), was calculated according to the formulas

$$E_{surf} = \frac{E_{Mg(0001)} - 54E_{Mg}}{2} \quad \text{and} \quad E_{surf} = \frac{E_{MgX(0001)} - 53E_{Mg} - E_X}{2}.$$

The surface energy of pure Mg(0001) was found as 0.56 J/m2, approximately 30% lower than the experimental value, as a result of general tendencies of GGA functionals to underestimate the metal surface energies. However, it is expected that the shortcoming of our functional does not cause a problem in evaluation of the surface energy change with

doping, considering that the doping concentration of X in Mg is low. It is found that doping of X=Al, Mn and Fe increases the surface energy of the Mg(0001), whereas X=Zn and Ca, in opposite, decrease it (Table 1).

Table 1. Surface energies of MgX(0001)

X	Mg	Fe	Mn	Al	Zn	Ca
E (J/m^2)	0.56	0.69	0.66	0.56	0.56	0.53

For adsorption of the H2O, OH and H, on pure and doped Mg(0001), all possible adsorption sites, composed of either pure Mg atoms, the single surface X atom, or a combination of Mg and X atoms are tried. Computations revealed that the presence of surface impurities can cause changes in the adsorption energies and configurations either directly, i.e. when the surface impurity atom binds the adsorbate, or through an indirect interaction in which the impurity changes the electronic and chemical properties of surface Mg atoms and consequently influences the H2O-Mg bonds, or a combination of thereof. The energetically most favored adsorption configurations for H2O, OH and H are given in Figures 2-4.

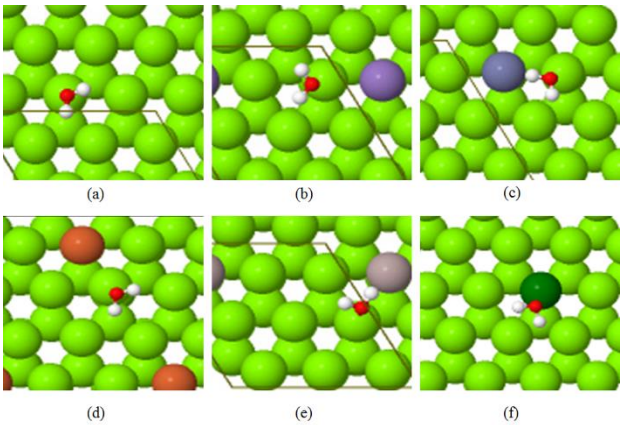

Figure 2. Most favorable adsorption site of H_2O on Mg-X(0001) with (a) X=Mg, (b) X=Mn, (c) X=Zn, (d) X=Fe, (e) X=Al and, (f) X=Ca.

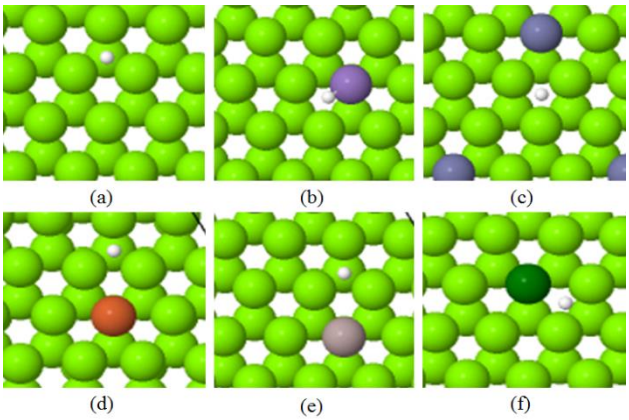

Figure 3. Most favorable adsorption site of H_2O on Mg-X(0001) with (a) X=Mg, (b) X=Mn, (c) X=Zn, (d) X=Fe, (e) X=Al and, (f) X=Ca.

In the case of H2O, computations revealed that presence of the impurity decreases the adsorption energy, i.e. increases the strength of H2O adsorption on the surface. Thus, the presence of H2O molecules on the surface is a driving force for the diffusion of the impurities from the bulk to the topmost layers.

In the case of H and OH, computations revealed that presence of the impurity decreases the adsorption energies, i.e. increases the strength of both OH and H adsorption on the surface. Computations overall indicate that impurity atoms on the surface, as well as the neighboring Mg atoms around them are active sites in conversion of H2O into OH and H.

In an electrochemical environment where water is present, the two reactions can proceed

Rxn 1. $H_2O_{ads} \rightarrow OH_{ads} + H^+(aq) + e^-$

Rxn 2. $H_2O_{ads} + e^- \rightarrow H_{ads} + OH^-(aq)$ or in acidic solutions, $H_3O^+(aq) + e^- \rightarrow H_2O_{ads} + H_{ads}$

The rate of the two reactions depend on the potential effective on the metal surface. The equilibrium potential (at which the reactions turn into exothermic) with respect to standard hydrogen electrode can be calculated with these two equations.

$$U_{Rxn1} = E_{H2O/MgX(0001)} - E_{OH/MgX(0001)} - 1/2E_{(H2,gas)} - \Delta ZPE_{Rxn1} - \Delta TS_{Rxn1}$$
$$U_{Rxn2} = E_{H/MgX(0001)} - 1/2E_{(H2,gas)} - E_{MgX(0001)} + \Delta ZPE_{Rxn2} + \Delta TS_{Rxn2}$$

For potentials below U_{Rxn2}, Rxn 2 becomes exothermic and thus Hads species is produced on the surface, which then react to form $H_{2,gas}$ through $2H_{ads} \rightarrow H_{2,gas}$.

At potentials from U_{Rxn2} to U_{Rxn1}, H_2O is stable, whereas at potentials higher than U_{Rxn1}, the metal surface is covered by OH_{ads} species, through Rxn 1.

Our computations on vibrational frequencies of adsorbate-metal systems to calculate the ΔZPE and ΔTS are in progress. Electronic energy computations that are completed up to now indicate: (i) As compared to the pure Mg(0001) equilibrium potential, the presence of impurities, as modeled by X=Al, Zn and Ca, show negligible influence on U_{Rxn1}, i.e. the potential dependent rate of surface OH_{ads} formation. (ii). U_{Rxn2}, i.e. the potential dependent rate of surface H_{ads} formation. On the other hand is affected by impurities. We computed a shift to cathodic potentials by ~0.1 V in the case of X=Al and Zn and by ~0.3 V in the case of X=Ca .

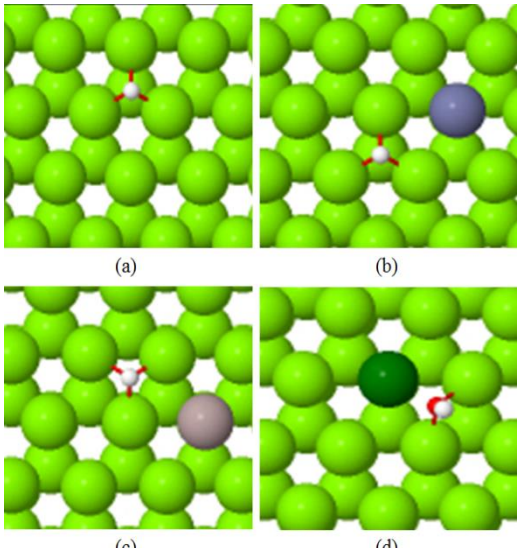

Figure 4. Most favorable adsorption site of OH on Mg-X(0001) with (a) X=Mg, (b) X=Zn, (c) X=Al and, (d) X=Ca.

4.2. Macroscale Corrosion Damage

For the development of the ISV corrosion modeling, the corrosion model was built upon the framework proposed by Walton [17], which was built upon Bammann [10, 18, 19] and Horstemeyer [15, 20]. The kinematics and thermodynamic formulations can be found in Walton [17], so no effort will be put forward in this report to rehash those aspects. Instead, an abbreviated version of the new macroscale damage formation is presented below. The full version of the formation can be found in Song [2015].

Damage parameter, ϕ, is used throughout the kinematic development as well as the plastic flow rule. In this section, a physically and phenomenological based model will be developed to capture the corrosion damage evolution. The total corrosion damage can be defined as

$$\phi_{total} = \phi_{gc} + \phi_{pc} + \phi_{ic} \tag{4.2.1}$$

where ϕ_{gc} is the general corrosion damage, ϕ_{pc} is the localized pitting corrosion damage, ϕ_{ic} is the intergranular corrosion damage. For different magnesium alloys, types of second phase particles, base materials' chemical composition, and microstructure features, will affect each type of corrosion damage differently. In addition, filiform corrosion may substitute intergranular corrosion occurring on the surfaces, at this situation, the ϕ_{ic} can be changed to ϕ_{fc} in Eq. (4.2.1). The associated damage rate equation is obtained as the following form

$$\dot{\phi}_{total} = \dot{\phi}_{gc} + \dot{\phi}_{pc} + \dot{\phi}_{ic} \tag{4.2.2}$$

Horstemeyer [15] developed an equation to account for the relative pitting corrosion damage

$$\phi_{pc} = \eta_p \nu_p c_p \tag{4.2.3}$$

Where η_p represents pit nucleation related to the pit number density, ν_p represents pit growth related to the pit in-plane area, pit depth, and pit volume, and c_p is the pit coalescence term related to the nearest neighbor distance between pits.

4.1.1. Macroscale General Corrosion rate

General corrosion can be referred to corrosion which attacks an exposed surface uniformly without inducing appreciable localization. General corrosion can be obtained by measuring the mass change or thickness change of the specimen. Faraday's law [27] proposed that the mass loss of an electrode during electrolysis is directly proportional to the quantity of electricity transferred at that electrode.

$$m = \frac{QM}{Fz} \tag{4.2.1.1}$$

where m is the mass change of an electrode in grams, Q is the total electric charge passed through the substance, F is the Faraday constant, M is the molar mass of the substance, z is the valency number of ions of the substance, $z = 2$ for magnesium. For the general corrosion rate, $\dot{\phi}_{gc}$, a modified Faraday's law was proposed

$$\dot{\phi}_{gc} = C_1\left(C_2 + \phi_{gc}\right)\frac{M}{FZ} \tag{4.2.1.2}$$

Where C_1 and C_2 are material parameters that are determined by the material properties.

4.1.2. Macroscale Pitting Corrosion

The pitting corrosion is a form of extremely localized corrosion that results in the creation of small holes in the metal. Pitting corrosion usually is defined as an autocatalytic process [28]. The spatial separation of the cathodic and anodic half-reactions generates a potential gradient and promotes the electromigration of aggressive anions into the pits, causing the pit nucleation, growth, and coalescence.

Pits are susceptible to nucleate at impurities, inclusions, grain boundaries, or surface defect/flaw regions, because these inhomogeneous sites can facilitate breakdown of the passive films [29]. The pit nucleation rate can be written as

$$\dot{\eta}_p = \begin{cases} C_3(C_4 - \eta) & \text{if } t < t_c \\ C_5(C_6 - \eta) & \text{if } t \geq t_c \end{cases} \tag{4.2.2.1}$$

where $C_3 - C_6$ are material parameters, that are as a function of second phase/particle volume fraction, particle size, temperature, pH level. t_c is the transition time from pit nucleation dominated to pit coalescence or general corrosion dominated.

The pit growth rate and stability of the active corrosion are dependent on material composition, aggressive electrolyte concentration, formation and dissolution of corrosion film, and the potential inside the pit [29, 30].

The pit growth equation is expressed as the following form

$$\dot{v}_p = \begin{cases} C_7(C_8 - v) & \text{if } t < t_c \\ C_9(C_{10} - v) & \text{if } t \geq t_c \end{cases} \tag{4.2.2.2}$$

where C_7 and C_8 are material parameters that change as a function of temperature, pH level, and materials microstructural characteristics. v is the average pit volume on the specimen surfaces, please note that v can also be the average in-plane pit area if you measured pit area instead of pit volume.

In real situations, pits will interact with neighboring pits and coalesce into larger pits. The coalescence rate, $\dot{C}$, is assumed to relate to the electrochemical interaction forces between pits. Walton [17] proposed a pit coalescence model based on the Coloumb's Law and Maxwell's stress. The original form of Coloumb's Law is

$$F_c = \frac{k_e q_1 q_2}{r^2} \tag{4.2.2.3}$$

where F_c is the electrostatic interaction force between pits, k_e is the Coulomb constant ($k_e = 8.987 \times 10^9\ \mathrm{Nm^2/C^2}$), q_1 and q_2 are point charges. r is the separation distance between two pits, will be defined as the nearest neighbor distance (NND) for corrosion pits. In combination both the Coulomb's Law and Maxwell stress together, we arrived at the following pitting coalescence rate.

$$\dot{c}_p = \frac{k_e q_1 q_2}{\varepsilon_0 \pi \left[\overline{N\dot{N}D}(t)\right]^4} \tag{4.2.2.4}$$

$$\dot{\overline{NND}} = \begin{cases} C_{11}(C_{12} - NND) & \text{if } t < t_c \\ C_{13}(C_{14} - NND) & \text{if } t \geq t_c \end{cases} \quad (4.2.2.5)$$

where ε_0 is the electric constant equal to 8.854×10-12 F/m and $C_{11} - C_{14}$ are material parameters.

4.1.3. Macroscale Intergranular Corrosion

Intergranular corrosion is localized attack along grain boundaries, or regions adjacent to the grain boundaries [31]. This form of corrosion mainly induced by the uneven distribution of the chemical composition, because impurities or second phases tend to form on the grain boundaries. The segregation of the chemical composition results in the formation of the galvanic cells along grain boundaries. The intergranular corrosion rate, ϕ_{ic}, is formulated as the following form

$$\dot{\phi}_{ic} = \begin{cases} C_{15}(C_{16} - \phi_{ic}) \left(\frac{MO}{MO_0}\right)^{z_{ic}} & \text{if } t < t_c \\ C_{17}(C_{18} - \phi_{ic}) \left(\frac{MO}{MO_0}\right)^{z_{ic}} & \text{if } t \geq t_c \end{cases} \quad (4.1.3.1)$$

where $C_{15} - C_{18}$ are material parameters, $(MO/MO_0)^{z_{ic}}$ is a is grain misorientation factor that represents galvanic cells formed. The misorientation factor, which describes the distribution of crystallographic orientation that can be obtained from the EBSD/pole figure results.

5.2. Mesoscale Electrochemical Kinetics

The Butler-Volmer equation describes the kinetics for electrochemical reactions is controlled by the transfer of charge across the interface [32, 33]. Butler-Volmer equation links four very important parameters together: Faradaic current, electrode potential, concentration of reactant, and concentration of product.

$$i = i_{corr} \left\{ \exp\left(\frac{\alpha_a n F_R}{RT} \Delta E\right) - \exp\left(-\frac{\alpha_c n F_R}{RT} \Delta E\right) \right\} \quad (4.1.3.1)$$

$$\Delta E = \left(E - E_{eq}\right) \quad (4.1.3.2)$$

The first term represents the anodic partial current density, and the second term is the cathodic partial current density [34]. Where i is the electrode current density, i_{corr} is the exchange current density, ΔE is the overpotential, E is the electrode potential, and E_{eq} is the equilibrium/reversible potential. From the above relationships, the net current (i) is positive when the electrode is polarized anodically and negative when the electrode is polarized catholically. n is the number of electrons involved in the electron reaction, F_R is the Faraday constant, R is the universal gas constant. α_a and α_c are the so-called anodic and cathodic charge transfer coefficient, respectively. Please note that the values of α_a and α_c do not necessarily sum to unity, but they are related by

$$\alpha_a + \alpha_c = \upsilon^{-1} \quad (4.1.3.3)$$

where υ is the stoichiometric number, or the number of times that the rate-determining step (RDS) must occur for the overall reaction to occur once.

When the anodic polarization potential is large enough from the equilibrium potential ($\eta_a > 50$ mV), the first term of the Eq. (4.1.3.1) dominates the second term. Thus, the Butler-Volmer equation can be simplified to

$$i = i_0 \exp\left(\frac{\alpha_a n F_R}{RT}\Delta E\right) \tag{4.1.3.4}$$

Equation (4.1.3.4) can be rearranged to get the Tafel equation as

$$\eta_a = \beta_a \log\left(\frac{i}{i_0}\right) \tag{4.1.3.5}$$

where β_a is the anodic Tafel slope. β_a can be associated with α_a in the following way.

$$\beta_a = \frac{2.3RT}{\alpha_a n F_R} \tag{4.1.3.6}$$

A similar equation is obtained for the cathodic activation polarization

$$\eta_c = -\beta_c \log\frac{|i|}{i_0} \tag{4.1.3.7}$$

where β_c is the cathodic Tafel slope, and it relates to α_c by

$$\beta_c = \frac{2.3RT}{\alpha_c n F_R} \tag{4.1.3.8}$$

According to the Stern-Geary equation [35], the exchange corrosion current can be determined by a small polarization from the corrosion potential.

$$i_{corr} = \frac{\beta_a \beta_c}{(\beta_a + \beta_c) + 2.3R_p} \tag{4.1.3.9}$$

where R_p is the polarization resistance, can be defined as the slope of the linear polarization curve at the corrosion potential. For our model, we regard R_p as material property, and it does not change over exposure time, note that the unit of R_p is $\Omega\ \mathrm{cm}^{-2}$. When substituting Eqs. (4.1.3.6, 4.1.3.8) into Eq. (4.1.3.9), one gets

$$i_{corr} = \frac{RT}{nF(\alpha_a + \alpha_c)R_p} \tag{4.1.3.10}$$

Substituting the exchange current Eq.(5.2.10) into the Butler-Volmer equation Eq.(5.2.4), the corrosion current can be changed to the following form.

$$i = \frac{RT}{nF(\alpha_a + \alpha_c)R_p} \exp\left(\frac{\alpha_a n F_R}{RT}\Delta E\right) \tag{4.1.3.11}$$

The corrosion current density, i, that determined from the electrochemical kinetic part, can be used to quantify the corrosion rate occurred on the surface. The rate of material loss, r ($\mathrm{g\ h}^{-1}$), is associated with the corrosion current density, i ($\mathrm{A\ cm}^{-2}$), by:

$$r = i\frac{M}{nF} \tag{4.1.3.12}$$

The corrosion current, i, is the sum of general corrosion current, i_{gc}, and pitting corrosion current, i_{pc}.

4.3 Microstructural Analysis

For multi-phase Mg alloys, the macroscale corrosion damages are affected by three important factors: (i) the chemical composition of each phase (ii) the fraction of each phase in the material (iii) the microstructural distribution of second phases in the material. For the casted Mg-Al alloys, eutectic α phase usually formed along dendritic arms or grain boundaries, it contained higher level of aluminum in the solid solution. β phase usually precipitates within the eutectic α phase, with the increase of aluminum content in material, β phase will precipitate more continuously along the grain boundaries and form finer lamellar arrangement. Figure 5.3.1 shows the distribution of the α, eutectic α, and β phases in the Mg-6Al magnesium alloy. As the eutectic α phase and β phase have lower corrosion rates than the α phase, they can improve the overall corrosion resistance of the material. On the other hand, because the eutectic α phase and β phase have more positive electrochemical potential, they can act as effective cathodic sites to matrix α phase and accelerate the dissolution rate of the α phase [36]. Therefore, in order to capture the corrosion behavior of Mg alloys accurately, we need to consider both the corrosion resistance improvement and anodic dissolution acceleration affected by the second phases.

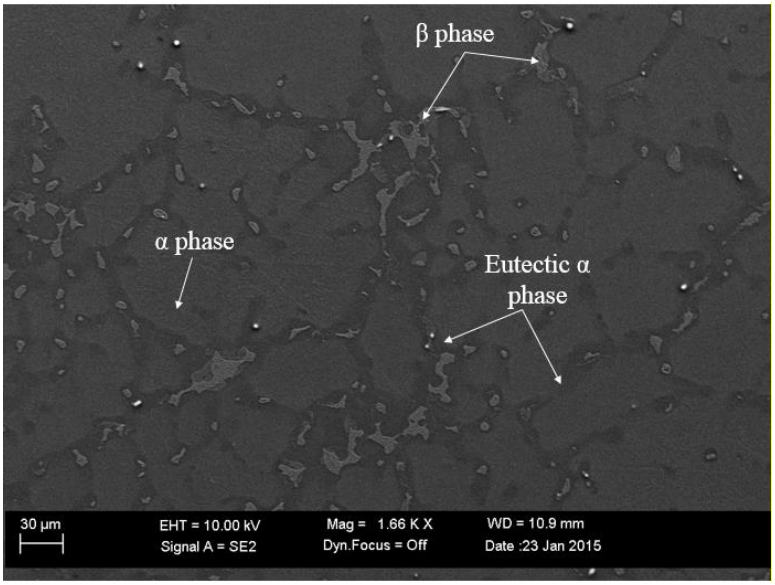

Figure 4.3.1. The distribution of the α, eutectic α, and β phases in the Mg-6Al alloy.

Liu [37] quantified the eutectic α phase and β phase (Mg17Al12) for Mg-Al alloys (Mg-0.5wt.% Al, Mg-1 wt.% Al, Mg-2 wt.% Al, Mg-4 wt.% Al, Mg-6 wt.% Al, Mg-9 wt.% Al, Mg-12 wt.% Al), it was found that the volume fraction and the size of both phases increased with the addition of aluminum content and almost followed a linear relationships. Actually, due to the different manufacturing process, such as, cooling rate and heat treatment, the microstructure for the same Mg alloys can be different. The casted Mg-Al alloys for this study were prepared with the same casting procedure, their microstructure features can be associated with the Al weight percentage, ξ, by the following form.

$$GS(\xi) = 370599\xi^2 - 37012\xi + 1025.8,$$
$$D_{Eu\,\alpha}(\xi) = 358.21\xi + 1.0318, \quad \delta_{Eu\,\alpha}(\xi) = 6903\xi + 7.6459 \tag{4.3.1}$$

$$NND_{Eu\,\alpha}(\xi) = 114.25\xi + 38.285, \quad f_{Eu\,\alpha}(\xi) = -3.407\xi + 0.4044 \tag{4.3.2}$$

$$P_{Eu\,\alpha}(\xi) = 25.012\xi^2 + 0.0993\xi + 0.002, \;\; P_{matrix}(\xi) = 0.5007,$$
$$D_{\beta}(\xi) = 1944\xi^2 - 20.223\xi - 0.0921, \tag{4.3.3}$$
$$\delta_{\beta}\,(\xi) = 41518\xi^2 - 446.9\xi - 443.926$$

$$NND_{\beta}(\xi) = -436.13\xi + 39.707, \;\; f_{\beta}\,(\xi) = 7.3 \times 10^{-6} \exp 145.3\xi, \tag{4.3.4}$$
$$E(\xi) = 1.667\xi + 1.663$$

where $GS(\xi)$ is the grain size (μm), $D_{Eu\,\alpha}(\xi)$ is the particle size/phase size (μm) of the eutectic α phase, $\delta_{Eu\,\alpha}(\xi)$ is the number density (mm^{-2}) of eutectic α phase, $NND_{Eu\,\alpha}(\xi)$ is the nearest neighbor distance (μm) of the eutectic α phase, and $f_{Eu\,\alpha}(\xi)$ is the area fraction of the eutectic α phase in the material. $P_{Eu\,\alpha}(\xi)$ is the aluminum content (wt.%) in the eutectic α phase, $P_{matrix}(\xi)$ is the aluminum content (wt.%) in the matrix material. $D_{\beta}(\xi)$, $\delta_{\beta}\,(\xi)$, $NND_{\beta}(\xi)$, and $f_{\beta}\,(\xi)$ are the particle size (μm) of β phase, particle number density (mm^{-2}) of β phase, nearest neighbor distance (μm) between β phase particles, and area fraction of β phase, respectively. $E(\xi)$ is the electrochemical potential value of Mg-Al solution phase. Song [2015] explains the link between the microstructure specific equations in Eqs. (4.3.1-4.3.4) and the corrosion equations.

5. Results and Discussion

The microstructural features such as, particle size, particle number density, nearest neighbor distance, aluminum content in each phase, grain size, and second phase area fraction were quantified for the casted pure Mg, Mg-2% Al, and Mg-6% Al alloys. Then, the microstructural characteristics and electrochemical potential of each phase were inputted into the multiscale ISV corrosion model, and the predicted corrosion process (general, pitting, and intergranular corrosion) are compared with the experimental data as shown in Figures 5.1–5.3. Good agreement was found between the model validation results and the experimental data.

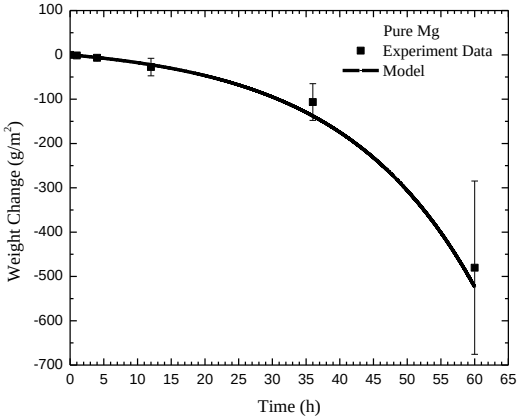

(a)

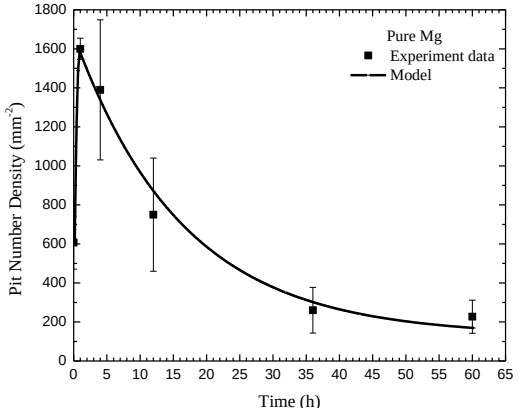

(b)

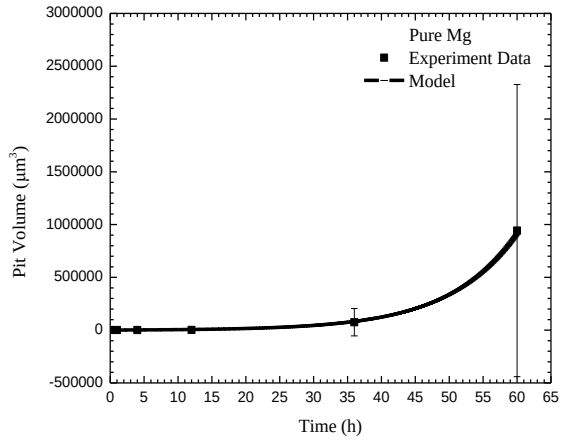

(c)

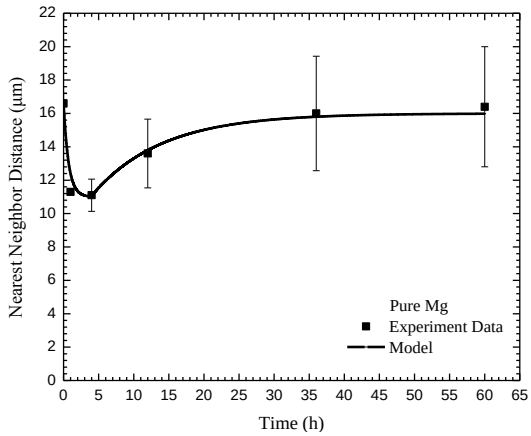

(d)

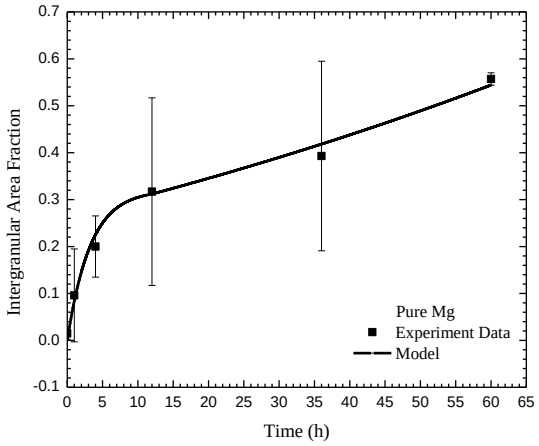

(e)

Figure 5.1. Comparison between the proposed theoretical damage framework and the corrosion experimental data of Pure Mg (3.5% wt.% NaCl immersion environment). Experimental data versus the model for (a) change in mass, (b) pit number density, (c) pit area fraction, (d) pit nearest neighbor distance, (e) intergranular corrosion area fraction. The error bars were one standard deviation in each direction

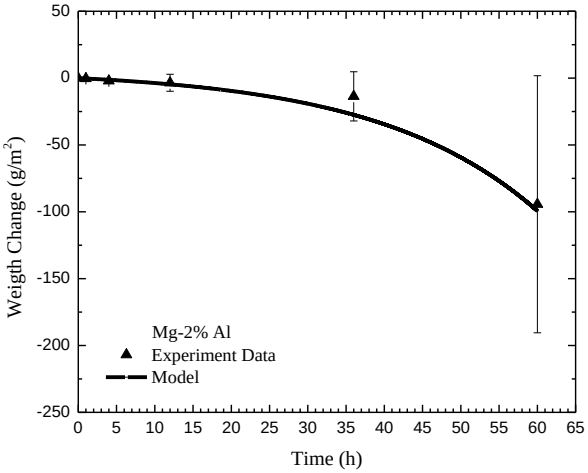

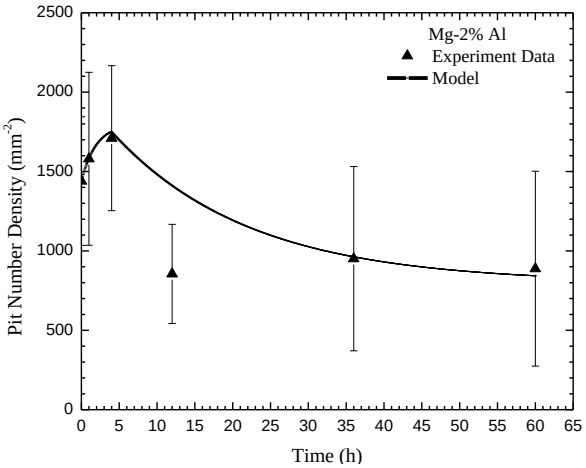

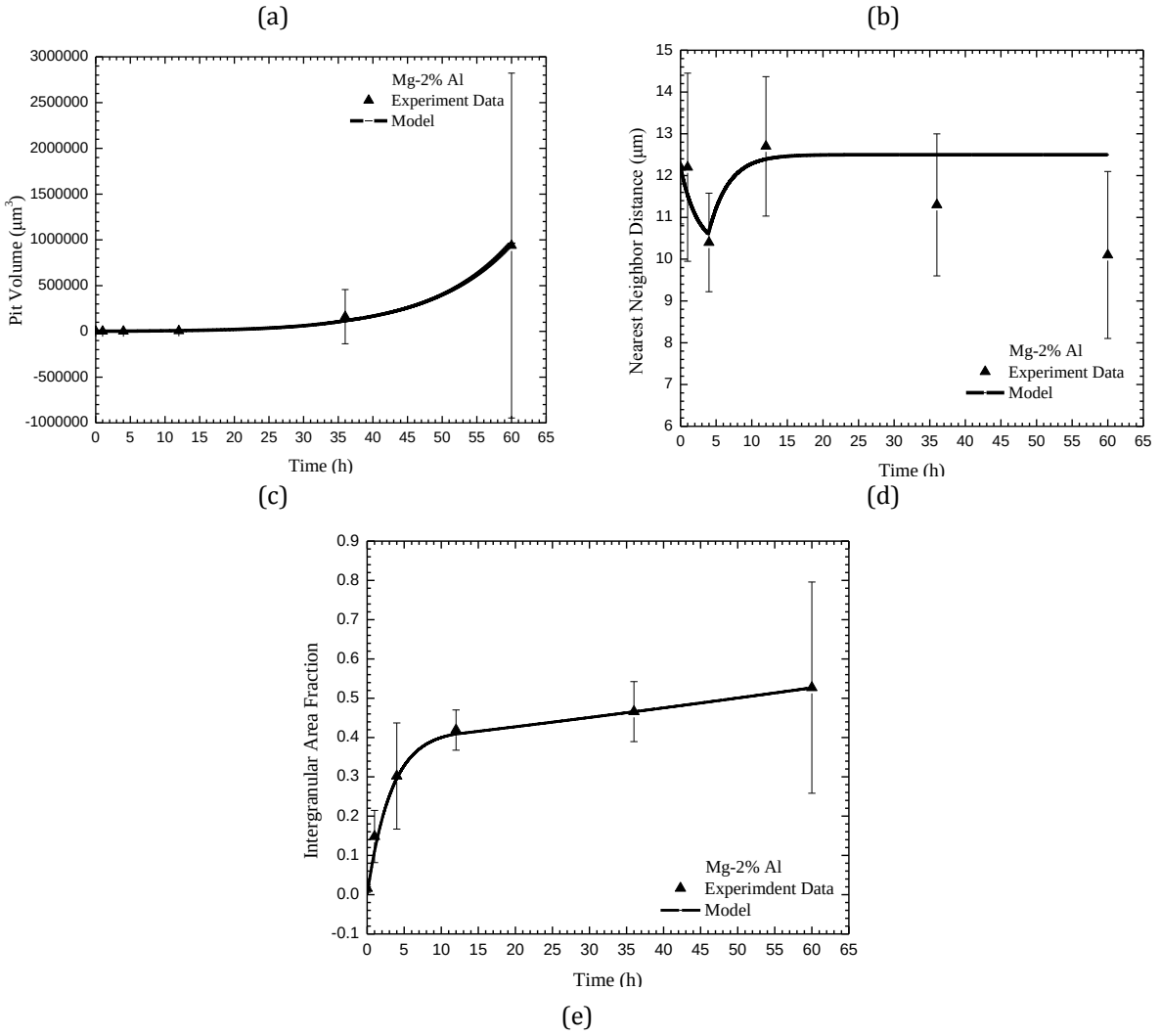

Figure 5.2. Comparison between the proposed theoretical damage framework and the corrosion experimental data of Mg-2% Al alloy (3.5% wt.% NaCl immersion environment). Experimental data versus the model for (a) change in mass, (b) pit number density, (c) pit area fraction, (d) pit nearest neighbor distance, (e) intergranular corrosion area fraction. The error bars were one standard deviation in each direction.

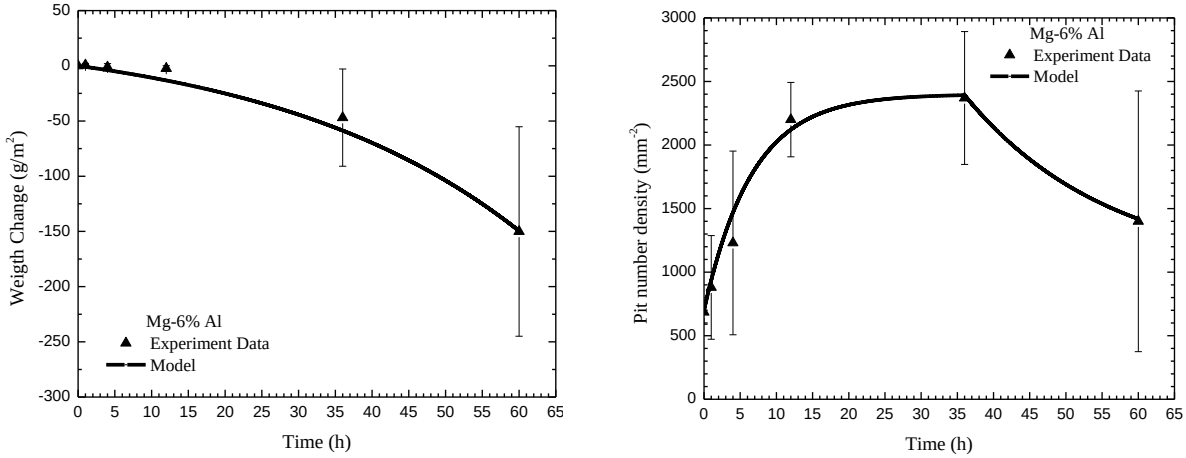

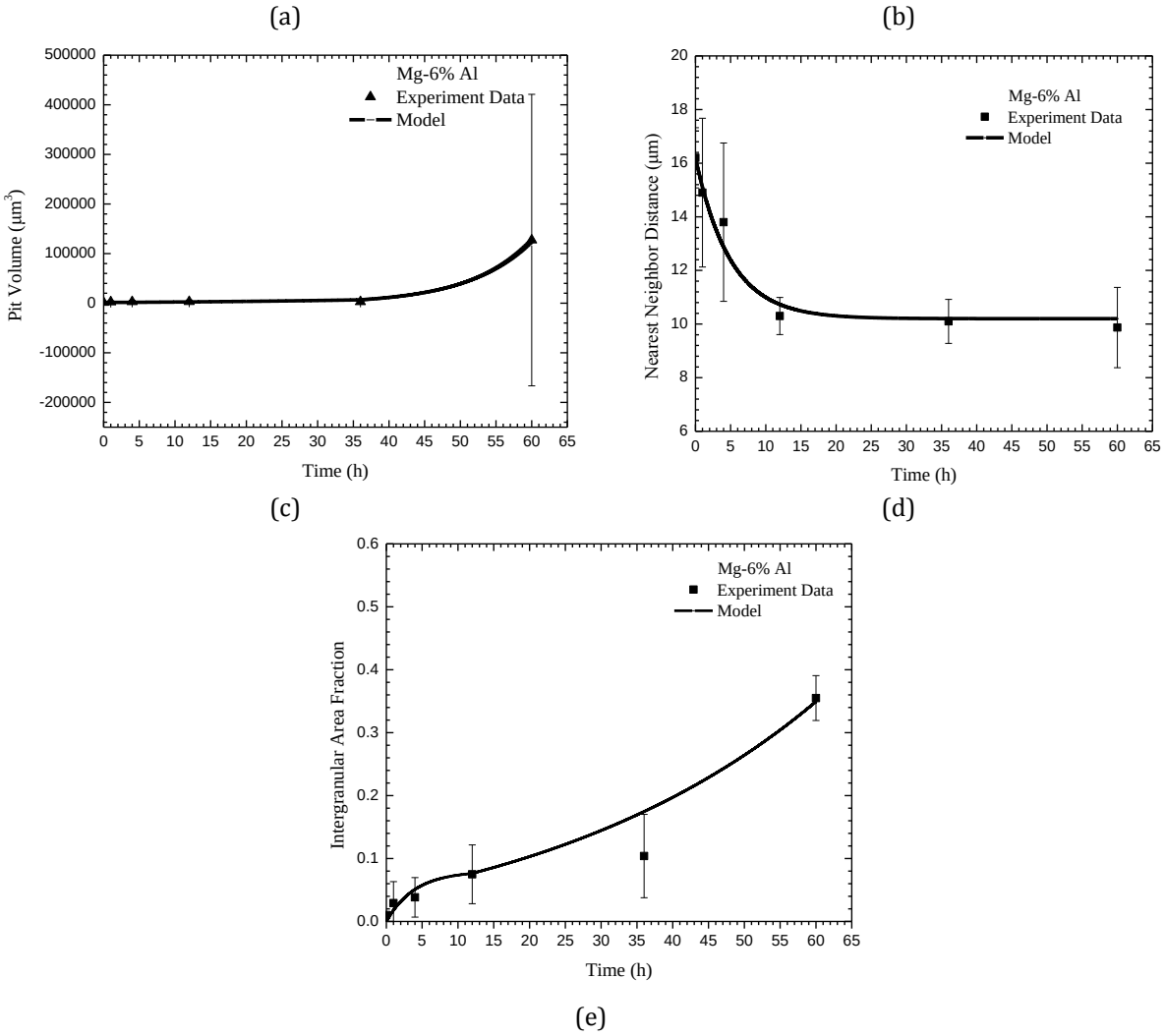

Figure 5.3. Comparison between the proposed theoretical damage framework and the corrosion experimental data of Mg-6% Al (3.5% wt.% NaCl immersion environment). Experimental data versus the model for (a) change in mass, (b) pit number density, (c) pit area fraction, (d) pit nearest neighbor distance, (e) intergranular corrosion area fraction. The error bars were one standard deviation in each direction.

6. Conclusion

DFT computations proved a strong influence of the second metal, e.g. Al, Ca, Mn, Fe, Zn, on the adsorption energetics of reactants, intermediates and products of hydrogen evolution on Mg. The findings point out changes in the potential dependent reaction rates due to the dopant presence on the surface. A multiscale corrosion constitutive model that joins the damage and mechanical effects for magnesium alloys has been developed. The kinematics, thermodynamics, and kinetics were considered in formulation of the internal state variables to account for different corrosion damage mechanisms, such as, general corrosion, pitting corrosion, and intergranular corrosion. The macroscale corrosion damage is bridged to the mesoscale electrochemical kinetics based on the Butler-Volmer equation, which is further

bridged to materials' microstructural properties. The theoretical framework of this model can be implemented to a finite element code in engineering analysis, as well as extended to include other kinds of damages occurred in the engineering field.

7. Presentations/Publications/Patents

Walton, C.A. , Horstemeyer, M.F., Martin, H.J., Francis, D.K.**, "** Formulation of a macroscale corrosion damage internal state variable model," *Int. Journal of Solids and Structures*, Vol. 51, Issue 6, 15, pp. 1235-1245, 2014.

Walton, C.A., Martin, H.J., Horstemeyer, M.F., Whittington, W.R., Horstemeyer, C.J., Wang, P.T.**,** "Corrosion stress relaxation and tensile strength effects in an extruded AZ31 magnesium alloy," *Corrosion Science*, Vol. 80, pp. 503-510, 2014.

Song, W. , Martin, H.J., Hicks, A., Seely, D., Walton, C.A., Lawrimore II, W.B., Wang, P.T., Horstemeyer, M.F., "Corrosion behaviour of extruded AM30 magnesium alloy under salt-spray and immersion environments," *Corrosion Science*, Vol. 78, Pages 353-368, 2014.

W. Song, H.J. Martin, M.Lugo, C. A. Walton, M.F. Horstemeyer, P.T. Wang, Corrosion Fatigue Behavior of an Extruded AM30 Magnesium Alloy in Sodium Chloride Solution Environment, The Minerals, Metals, and Materials Society Annual Meeting and Exchange, San Diego, California, Feb 15- Feb 21, 2014.

Song, Martin, Lugo, Lawrimore, Walton, Hughes, Brauer, HorstemeyerAM30 corrosion-fatigue paper (submitted Sept 2015) 90% completed

Song, Walton, Nouranian, Chaudhuri, Francis, Horstemeyer, Multiscale Internal State Variable Corrosion Cracking (to be submitted)

Santanu Chaudhuri, Ashley Summer, Weiwei Song, Mark Horstemeyer, DFT calculations (to be submitted)

Francis, D.L., Song, W.W., Horstemeyer, MF, "Completed chemothermomechanical damage model" (to be submitted)

8. References

[1] M. Rodríguez, Anticipated Degradation Modes of Metallic Engineered Barriers for High-Level Nuclear Waste Repositories, JOM, 66 (2014) 503-525.

[2] M. Caro, K. Woloshun, F. Rubio, S.A. Maloy, P. Hosemann, Heavy Liquid Metal Corrosion of Structural Materials in Advanced Nuclear Systems, JOM, 65 (2013) 1057-1066.

[3] T. Perez, Corrosion in the Oil and Gas Industry: An Increasing Challenge for Materials, JOM, 65 (2013) 1033-1042.

[4] B. Gordon, Corrosion and Corrosion Control in Light Water Reactors, JOM, 65 (2013) 1043-1056.
[5] S.A. Khan, Y. Miyashita, Y. Mutoh, Z.B. Sajuri, Influence of Mn content on mechanical properties and fatigue behavior of extruded Mg alloys, Materials Science and Engineering: A, 420 (2006) 315-321.
[6] C.A. Walton, H.J. Martin, M.F. Horstemeyer, P.T. Wang, Quantification of corrosion mechanisms under immersion and salt-spray environments on an extruded AZ31 magnesium alloy, Corrosion Science, 56 (2012) 194-208.
[7] M.F. Horstemeyer, D.J. Bammann, Historical review of internal state variable theory for inelasticity, International Journal of Plasticity, 26 (2010) 1310-1334.
[8] B.D. Coleman, M.E. Gurtin, Thermodynamics with Internal State Variables, The Journal of Chemical Physics, 47 (1967) 597-613.
[9] A.L. Gurson, Continuum Theory of Ductile Rupture by Void Nucleation and Growth: Part I—Yield Criteria and Flow Rules for Porous Ductile Media, Journal of Engineering Materials and Technology, 99 (1977) 2-15.
[10] D. Bammann, M. Chiesa, M. Horstemeyer, L. Weingarten, Failure in ductile materials using finite element methods, Structural crashworthiness and failure, (1993) 1-54.
[11] A.C.F. Cocks, M.F. Ashby, Intergranular fracture during power-law creep under multiaxial stresses, Metal Science, 14 (1980) 395-402.
[12] G.Z. Voyiadjis, B. Deliktas, Formulation of strain gradient plasticity with interface energy in a consistent thermodynamic framework, International Journal of Plasticity, 25 (2009) 1997-2024.
[13] G.Z. Voyiadjis, R.J. Dorgan, Framework using functional forms of hardening internal state variables in modeling elasto-plastic-damage behavior, International Journal of Plasticity, 23 (2007) 1826-1859.
[14] G.Z. Voyiadjis, P.I. Kattan, A plasticity-damage theory for large deformation of solids—I. Theoretical formulation, International Journal of Engineering Science, 30 (1992) 1089-1108.
[15] M. Horstemeyer, J. Lathrop, A. Gokhale, M. Dighe, Modeling stress state dependent damage evolution in a cast Al–Si–Mg aluminum alloy, Theoretical and applied fracture mechanics, 33 (2000) 31-47.
[16] M.F. Horstemeyer, A.M. Gokhale, A void–crack nucleation model for ductile metals, International Journal of Solids and Structures, 36 (1999) 5029-5055.
[17] C.A. Walton, M.F. Horstemeyer, H.J. Martin, D.K. Francis, Formulation of a macroscale corrosion damage internal state variable model, International Journal of Solids and Structures, 51 (2014) 1235-1245.
[18] D.J. Bammann, A model of crystal plasticity containing a natural length scale, Mater. Sci. Eng., (2001) 406–410.
[19] D.J. Bammann, G.C. Johnson, Modeling large deformation and failure in manufacturing processes, in: T. Tatsumi, E. Wanatabe, T. Kambe (Eds.), Theor. Appl. Mech., Elsevier Science, (1996) pp. 359–376.
[20] M.F. Horstemeyer, Integrated Computational Materials Engineering (ICME) for Metals: Using Multiscale Modeling to Invigorate Engineering Design with Science, John Wiley & Sons, (2012).
[21] B.D. Coleman, Gurtin Thermodynamics with internal state variables, Journal of Chemical Physics 47 (1967).

[22] M. Gurtin, An Introduction to Continuum Mechanics, Academic Press, San Diego, CA., (1981).
[23] D.J. Bammann, A damage model for ductile metals, Nucl. Eng., 116 (1989) 355–362.
[24] D.K. Francis, J.L. Bouvard, Y. Hammi, M.F. Horstemeyer, Formulation of a damage internal state variable model for amorphous glassy polymers, International Journal of Solids and Structures, 51 (2014) 2765-2776.
[25] L.E. Malvern, Introduction to the Mechanics of a Continuous Medium,, PrenticeHall, Inc., Englewood Cliffs, NJ, (1969).
[26] B.D. Coleman, Noll, W, Thermodynamics with internal state variables, Archive for Rational Mechanics and Analysis 4(1959) 97–128.
[27] R.G. Ehl, A.J. Ihde, Faraday's electrochemical laws and the determination of equivalent weights, Journal of Chemical Education, 31 (1954) 226.
[28] ASM Handbook, Volume 13, "Corrosion", ISBN 0-87170-007-7, ASM International, 1987.
[29] L. Zhu, STUDY OF CORROSION PITS IN CHLORIDE SOLUTION, University o f Illinois, PhD Thesis, (2002).
[30] P. Ernst, R.C. Newman, Pit growth studies in stainless steel foils. I. Introduction and pit growth kinetics, Corrosion Science, 44 (2002) 927-941.
[31] C.S. Tedmon, D.A. Vermilyea, J.H. Rosolowski, Intergranular Corrosion of Austenitic Stainless Steel, Journal of The Electrochemical Society, 118 (1971) 192-202.
[32] J. A. V. Butler, Trans. Faraday Soc., 19, 729-733 (1924).
[33] T. Erdey-Grúz and M. Volmer, Z. Physik. Chem., 150, 203-213 (1930).
[34] V. Encyclopedia of Electrochemistry, Corrosion and Oxide Films.
[35] M. Stern, A.L. Geary, Electrochemical Polarization: I . A Theoretical Analysis of the Shape of Polarization Curves, Journal of The Electrochemical Society, 104 (1957) 56-63.
[36] G. Song, A.L. Bowles, D.H. StJohn, Corrosion resistance of aged die cast magnesium alloy AZ91D, Materials Science and Engineering: A, 366 (2004) 74-86.
[37] M. Liu, P.J. Uggowitzer, A.V. Nagasekhar, P. Schmutz, M. Easton, G.-L. Song, A. Atrens, Calculated phase diagrams and the corrosion of die-cast Mg–Al alloys, Corrosion Science, 51 (2009) 602-619.
[38] Z. Shi, M. Liu, A. Atrens, Measurement of the corrosion rate of magnesium alloys using Tafel extrapolation, Corrosion Science, 52 (2010) 579-588.
[39] K.B. Deshpande, Numerical modeling of micro-galvanic corrosion, Electrochimica Acta, 56 (2011) 1737-1745.